JOURNAL OF MATERIALS SCIENCE 23 (1988) 1042–1049

Microanalysis of the surface in glass-ceramics obtained from muscovite–amblygonite

J. Má RINCÓN, P. CALLEJAS
Instituto de Cerámica y Vidrio, CSIC, Arganda del Rey, Madrid, Spain

A new family of glass-ceramics obtained from muscovite–amblygonite mixtures showing a schiller effect or reflecting surface has been obtained. This effect has not been observed in the bulk material. The raw materials contain about 1% iron as Fe^{2+}. In order to elucidate the correlation between surface structure and/or composition and the schiller surface effect, several surface analysis methods, (ESCA, RBS, EPR and reflection Mössbauer spectroscopy) have been used. It seems that a solid solution of Fe^{3+} in the spodumene crystal lattice precipitated from the surface is related to the reflecting effect, which can be controlled by solution of iron oxides in the β-spodumene solid solution.

1. Introduction

The preparation of glass-ceramics with a reflecting surface like a metal coating has been reported recently by Rincón *et al* [1, 2] from minerals such as muscovite, lepidolite, vermiculite and amblygonite.

The reflecting schiller or iridescent surface of this type of material can be due to different reasons:

(a) metal precipitation on the surface;

(b) unusual surface crystallization as very thin plates;

(c) aventurine effect produced by precipitation of very small crystals of magnetite or haematite, or

(d) solid solution of the Fe^{3+} and/or Fe^{2+} in the spodumene lattice crystallized on the surface by thermal treatment from the original glasses. The application of physico-chemical methods for surface studies such as electron spectroscopy for chemical analysis (ESCA), Rutherford backscattered spectroscopy (RBS), electronic paramagnetic resonance (EPR), and reflection Mössbauer spectroscopy, could enable us to determine the nature and mechanism of production of this type of glass-ceramic is with a homogeneous schiller effect on surface. Therefore, the aim of this paper was to elucidate the chemical and physical nature of this reflecting surface using these techniques.

2. Materials and methods

2.1. Materials

Four series of glasses have been prepared as indicated in Table I of [2], by melting in Si–Al crucibles in a propane gas furnace. No devitrification was observed, but by thermal treatment in the 600 to 800° C range, glasses and crystallized glass-ceramics with different crystalline volume fractions have been obtained. The glasses were annealed to release glass stresses prior to the thermal treatment for crystallization. The resulting glass-ceramics show a reflecting surface, like a metal coating.

The raw materials used were: muscovite from a kaolin laundry in La Coruña, Spain and an amblygonite from Cáceres, Spain.

2.2. Methods

2.2.1. Electron spectroscopy for chemical analysis (ESCA)

ESCA, also known as X-ray photoelectron spectroscopy (XPS) is a non-destructive method for surface analysis useful for all elements of the Periodic Table, with the exception of hydrogen. It allows us to detect chemical changes, element oxidation level, coordination number, type and characteristics of bonding, coupling spin-orbit, etc. It is also possible to perform depth analysis up to 3 nm from the surface.

Therefore, ESCA is a powerful tool not only for analytical purposes but also for investigating the electronic structure of solids. It could be also demonstrated that this method is well suited to distinguishing between the structural states of oxygen atoms in crystalline materials as well as in glasses. Discrimination is possible between O1s photoelectrons from network-forming and network-modifying oxygen atoms in alkali silicate, alkali phosphate and aluminosilicate glasses [3].

The objective of the analysis was to determine the chemical composition at the surface and at deeper levels. As ESCA only provides information from a depth of 1 to 3 nm it was necessary to remove sample material by ion bombardment. A UHV-chamber of the Perkin–Elmer, physical electronics ESCA/SAM spectrometer PHI model 560 System was used (scanning Auger-/ESCA-spectrometer).

Before the data were taken the sample was placed precisely in the focus point of the analyser. In this position we received the highest intensity of the ESCA analysis. The ion beam of the sputter source is also aligned to that point. Under these experimental conditions we achieved ESCA depth information with no crater-edge effects. The dimensions of the sputter crater were 4 mm × 4 mm and the acceptance area of the analyser has a spot size of 3 mm diameter. The ESCA spectra were generated with a Mg$K\alpha$ X-ray source.

0022–2461/88 $03.00 + .12

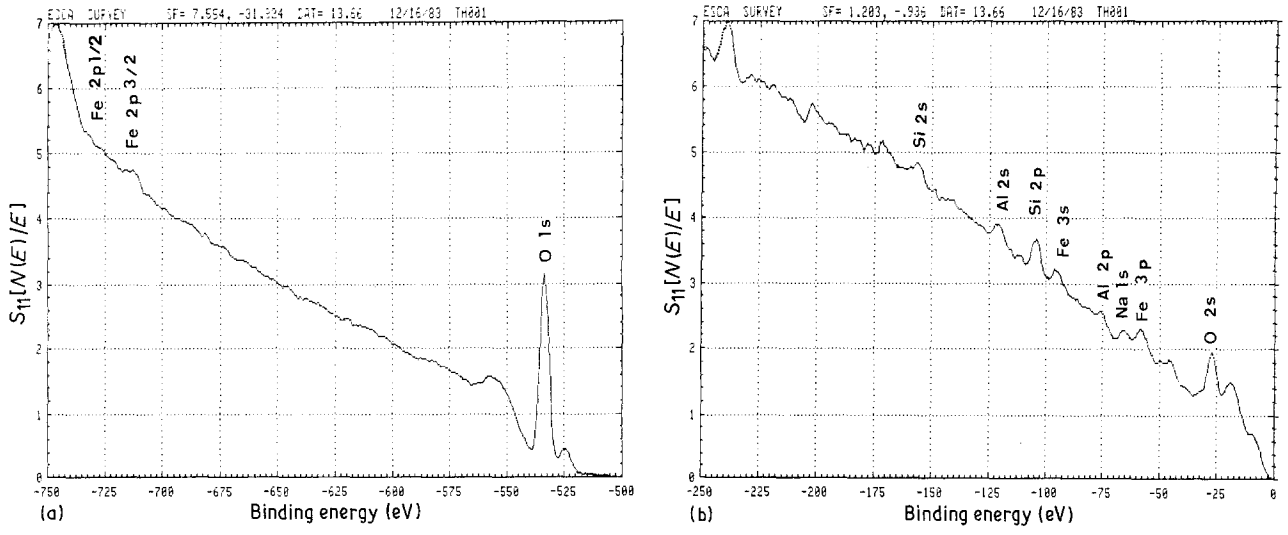

Figure 1 ESCA spectra on the surface of the original sample of the Ma5 glass-ceramic obtained by thermal treatment at 600° C for 16 h: (a) spectrum between −750 and −500 eV, and (b) spectrum between −250 and 0 eV.

2.2.2. Rutherford backscattered spectroscopy (RBS)

RBS consists of bombarding a sample with high-energy helium ions (He^{2+}, 2 MeV), measuring the energy of helium particles that are elastically back-scattered from the sample nuclei. RBS is a high-energy ionic beam analytical technique used for depth analysis of the material surface [4]. It can be used to characterize the phase-boundary layer between substrate and coating. It is a non-destructive method, with 1 to 3% accuracy. The most interesting feature is that it is the only spectrometric technique that does not require standardization, being independent of the nature of the matrix.

RBS is ideally suited to analysis of heavy material on a light substrate.

In a backscattered spectrum, the peak area (counts/sec) is directly proportional to a directly calculable scattering cross-section and to the number of analysed atoms present, matrix effects being unimportant.

A 4175 RBS model of General Ionex Corp. has been used for analysing the surface of muscovite–amblygonite transparent glass and the corresponding glass-ceramic. The He^{2+} ions are produced with an initial energy of 20 keV in an ion source which is external to the accelerator structure. The charge on these particles is then changed by a lithium charge exchange canal. They then are injected into the Taudetron accelerator and attracted to the positive 660 kV terminal achieving an energy of 680 keV. Later, their charge is changed by losing electrons. These He^{2+} ions are repelled from a positive terminal, accelerated again by an additional 1.32 MeV.

Therefore, an ion beam of $1.32 \pm 0.68 = 2.00$ MeV is directed on to the sample for RBS analysis. Finally, a solid state energy detector coupled to a multi-channel analyser was used to measure the energy and yield of the backscattered helium ions [4].

The RBS operation conditions in the experiments described here were: beam current of 50 μA; spot size 2 mm^2; beam energy 2 MeV. The mean acquisition time of the spectra was 15 min. The depth resolution was $\pm$ 10 nm and the depth profile analysis 10^5 nm. The specimen size was 10 mm × 10 mm × 1 mm.

2.2.3. Electronic paramagnetic resonance (EPR)

EPR is based on the transitions induced between different levels of a material with an odd number of electrons subjected to a magnetic field. The application of EPR to solids, crystalline or amorphous materials, gives us information on substitutional impurities such as transition metal ions or rare earths and radiation-induced centres [5]. The first EPR observations in glasses were carried out by Sands [6]. For EPR analysis a Bruker-220 spectrometer was used in this case.

2.2.4. Reflection Mössbauer spectroscopy

Reflection Mössbauer spectroscopy or conversion electron Mössbauer spectroscopy (CMES) has been widely described in the literature [7] and enabled us to determine the iron oxidation state. The Mössbauer spectra were obtained at ambient temperature in a conventional spectrograph with constant acceleration equipped with a ^{57}Co source embedded in palladium [8]. The experimental spectra were adjusted to a sum of lorentzian curves using a calculation program. The adjustment was carried out with the restriction of equal width (r) and equal lorentzian area of the two doublet lines, and on the magnetic sextetes the condition of equal line width on the six peaks and areas of the 1–2–3–3–5–6 lines in the 3 : 2 : 1 : 1 : 2 : 3 relation has been established. The relative concentration of different sites of iron has been calculated from the area relation of corresponding lorentzians.

For the CMES and electron counter of parallel plates conversion, built in the laboratory according to the Weyer design, has been used [9]. The material was melted in a mould with dimensions of the counter cathode and the surface was coated with a carbon film of 20 μg cm^{-2} (Yissum Research Development Co., Israel) equivalent to one-fifth of the maximum energy conversion electron ($\simeq$ 7 keV).

3. Results

3.1. ESCA analysis

Fig. 1 shows the ESCA (XPS) analysis of the sample Ma5 heat treated at 600° C for 16 h depicting a severe contamination with a hydrocarbon layer with oxygen

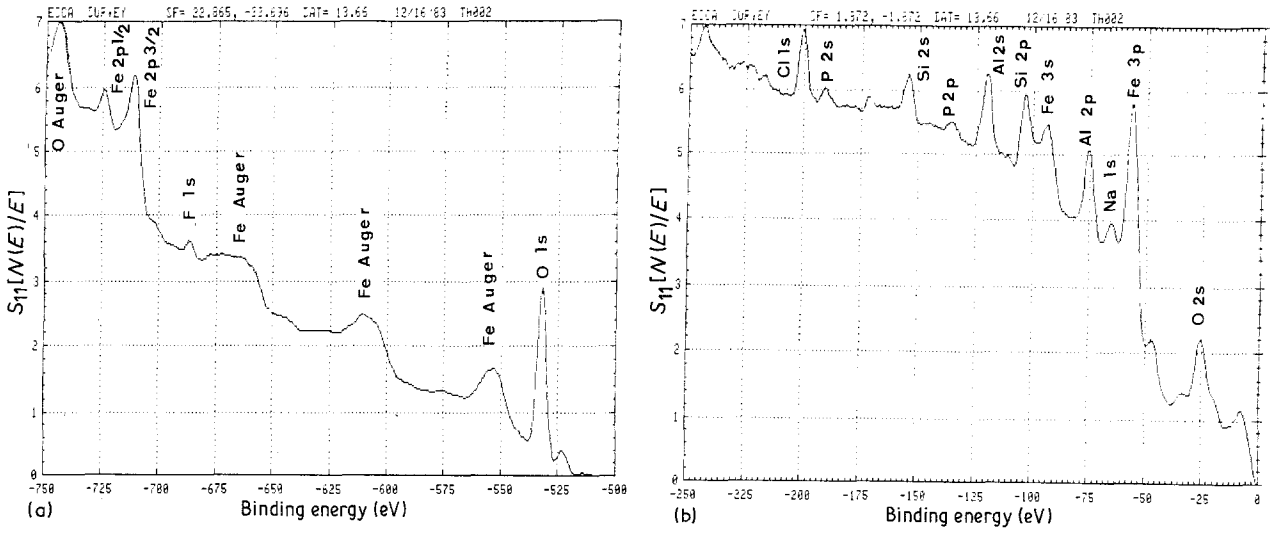

Figure 2 ESCA spectra after removal of 3 nm layer of the same glass-ceramic as Fig. 1: (a) spectrum between −750 and −500 eV, and (b) spectrum between −250 and 0 eV.

and calcium. Some traces of aluminium, iron, silicon and sodium are also visible.

After removal of a 3 nm layer by argon ion sputtering the carbon contamination decreased and the iron peaks become pronounced. Sodium and chlorine were identified as additional contaminants. Phosphorus, silicon and iron also became visible (Fig. 2). A further sputtering step to a depth of 6 nm reduced the carbon peak and enhanced the iron oxide concentration (Fig. 3). The absence of some containing elements of this material, such as lithium and potassium is due to the impact effect of the sputtering argon ions. They move the light highly mobile alkali cation into deeper layers.

Therefore, ESCA surface and depth analyses show that the glass composition close to the schiller surface is significantly different from the bulk composition. Iron oxide has been significantly enriched up to a concentration of ~50%. Al_2O_3 is close to bulk composition and SiO_2 and P_2O_5 are decreased. The sodium signal is due to surface contamination. It diffuses very rapidly and could be identified even after sputtering. Table I shows the composition (at. %) of the surface layers deduced from the ESCA results.

3.2. RBS analysis

Figs 4a and b show the RBS spectra obtained from both sides of a transparent glass-ceramic Ma5 with a reflecting or schiller surface. It can be seen that the reflecting surface shows a higher iron RBS peak (~300 channel) which does not appear at the back surface. Similarly, Figs 5a and b show the RBS spectra of a corresponding opaque glass-ceramic. Here too the reflecting surface is enriched in iron. Otherwise, calcium and copper peaks are visible in the reflecting surface spectrum. Table II gives the element content (at.%) obtained from both surfaces of the glass-ceramics considered here. The results obtained by ESCA are corroborated by RBS, i.e. the iron enrichment at the reflecting surface. The oxygen contents lie in the range of the bulk composition obtained by chemical analysis [2] but phosphorus is deficient on the schiller or reflecting surface. Likewise, silicon is in general lower than in the bulk sample chemically

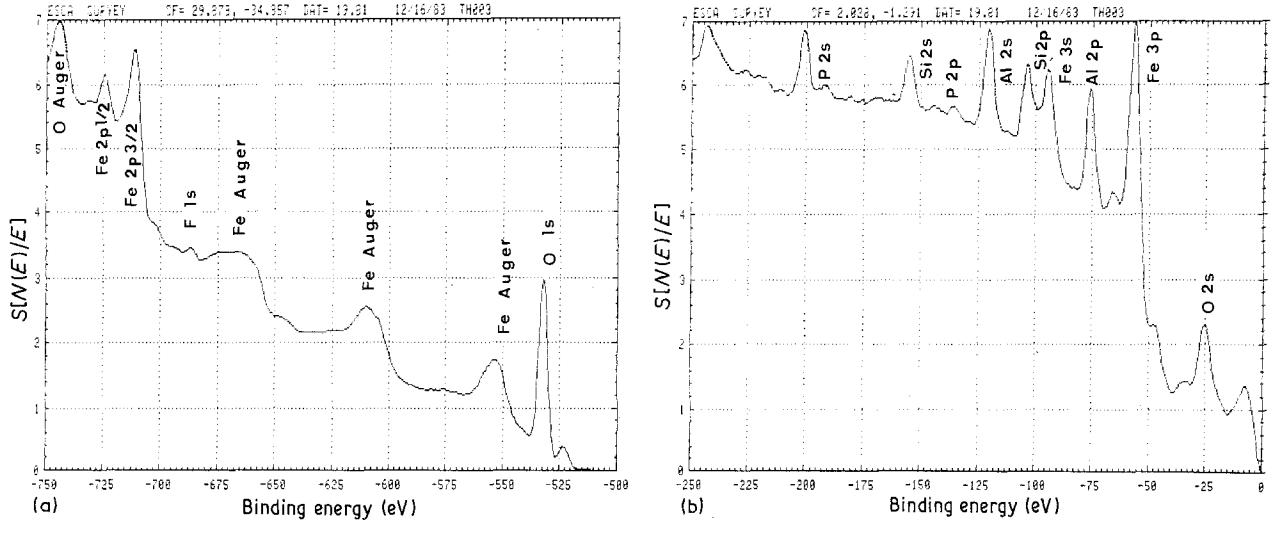

Figure 3 ESCA spectra after removal of 6 nm layer of the same glass-ceramic as Fig. 1: (a) spectrum between −750 and −500 eV, and (b) spectrum between −250 and 0 eV.

TABLE I ESCA (XPS) analyses on the surface of the Ma5/600/16 glass-ceramic with MgO addition

	Element (at. %)										
	C	N	O	Na	Al	Si	Mg	Ca	Fe	Mn	Ti
Original surface	65.7	1.3	21.5	–	2.87	7.7	–	0.4	0.5	–	–
Sputtered 30 min	22.3	0.8	41.2	0.1	?	1.0	3.1	0.4	16.3	1.9	0.2
Sputtered 60 min	13.0	0.2	55.1	–	15.9	1.8	5.8	0.4	21.5	2.8	0.5

analysed and may be due to the RBS peaks overlapping between silicon and aluminium [4]. In the same way, potassium and calcium show RBS overlapping that can produce a deficient potassium content and conversely an enhanced calcium content. Some copper could come from the brass mould or the specimen holder. Radon detected in the RBS analysis could be due to noble gas impurities associated with the He^{2+} bombardement ions.

In any case, the most prominent result obtained by RBS is the iron enrichment of the schiller or reflecting surface of the glass-ceramics obtained from muscovite–amblygonite.

3.3. EPR analysis

Figs 6a to d show the EPR spectra of the glass-ceramics considered with and without nucleating agents. All samples show similar bands, though with important differences in intensities of certain species.

The g-factor values corresponding to the narrow band at a wavelength of 1600 nm are related to the Fe^{3+} in tetrahedral positions. This narrow EPR emission does not appear in the Ma5 glass-ceramic containing no nucleating agent. However, the wide band appearing at 3200 nm can correspond to Mn^{2+} and/or Fe^{3+} in the octahedral position, but showing hyperfine structure with the nucleating agents TiO_2, MgO or ZrO_2 added to the original glass. This band is, in any case, more intense at the surface than in the bulk sample, indicating that the surface is enriched in Fe^{3+} in octahedral sites. With nucleating agents the difference between the surface and the bulk is less drastic being most similar to ZrO_2 addition.

The Ma5 glass-ceramic containing no nucleating agent and heat treated at 750° C for 2 h shows a peak area ratio $Fe^{3+}/Fe^{2+} = 25$ with respect to the bulk of the sample. This relation decreases to 4.3 in similar materials with TiO_2 addition, its value is 1.9 when MgO is added and finally, 1.5, when $ZrSiO_4$ is added. Table III contains these values.

This result demonstrates that iron is present on the surface mainly as Fe^{3+} but reducing progressively to Fe^{2+} with the additives tested here. In fact, it can be stated that the segregation process of Fe^{3+} is controlled, because increasing crystallization decreases the time available for Fe^{3+} and Fe^{2+} segregation. This ion separation effect in the crystalline phases can correspond to the solid solution series of iron in β-spodumene being lower, according to the EPR results, in the following sequence: $TiO_2 > MgO > ZrO_2$.

3.4. Reflection Mössbauer spectroscopy analysis

The spectra obtained for bulk samples by transmission and by reflection Mössbauer spectroscopy are shown in Figs 7a and b, respectively.

The experimental spectra have been conformed to lorentzian curves whose areas are related to the concentrations of each cation species. The form of these curves shows three species of iron: Fe^{2+} (A site), Fe^{2+} (B site) and Fe^{3+} (C site), being Fe^{2+} in octahedral and tetrahedral coordination, and Fe^{3+} in octahedral coordination. In no case was elemental iron detected; therefore, the element iron was not present on the surface of these glass-ceramics.

Table IV shows the values of Mössbauer parameters (QS/quadrupole splitting and IS interband splitting) corresponding to these iron species with their relative contents.

The reflection spectra obtained at the surface are

TABLE II RBS analyses of the surface (reflecting and back surface) of transparent and opaque glass-ceramic

Glass-ceramic	Element (at. %)										
	O	P	Al	Si	K	Ca	Fe	Cu	Rn	Te	Sr
Chemical analysis	51	11.7	19.6	14.3	2.1	–	1.3	–	–	–	–
Transparent											
reflecting surface											
30 nm	27.8	6.9	13.9	13.9	–	2.8	34.7	–	0.055	–	–
bulk	58.1	5.1	23.2	9.3	–	4.2	–	–	0.046	0.023	0.035
back surface	56.7	7.9	22.7	9.1	2.7	–	–	–	0.045	0.023	0.034
Opaque											
reflecting surface											
70 nm	50.4	–	18.3	–	–	2.3	26.4	2.5	0.057	–	–
bulk	61.7	3.8	29.8	–	–	2.6	–	–	0.053	0.02	0.032
back surface	61.8	8.2	16.5	–	–	2.5	0.4	0.21	0.041	–	0.062

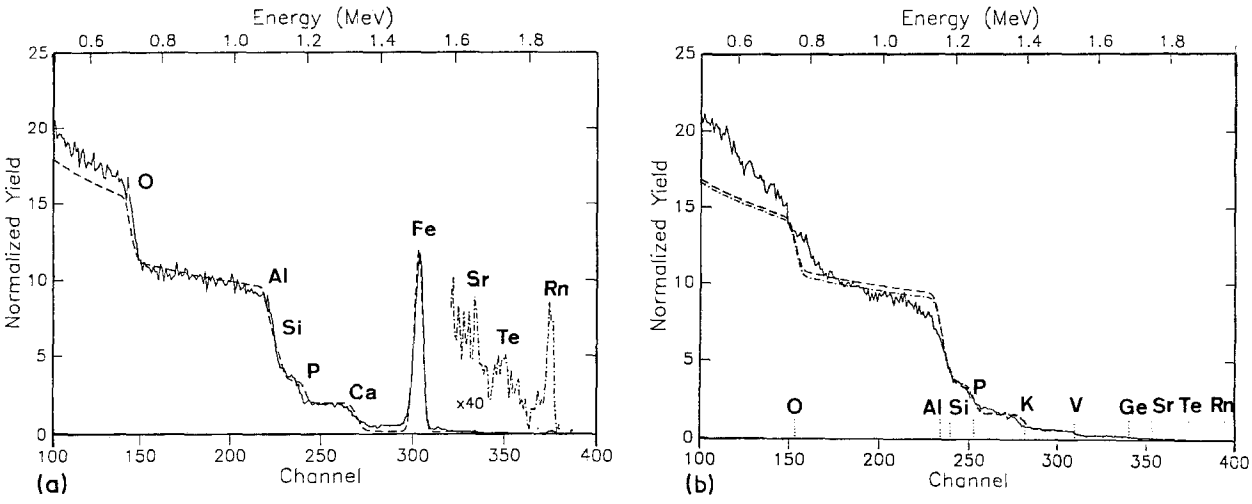

Figure 4 RBS spectra of the transparent original Ma2 glass: (a) reflecting surface, and (b) back-surface, whose reflecting surface was removed by grinding. (a) (——) Instituto de Ceramica, transparent, gic 01-05, (– – –) simulation of Fe–O–Al–Si–P–Ca–Rn/O–Al–Si–P–Ca–Rn–Te–Sr. (b) (——) Instituto de Ceramica, transparent, gic 01-07, (– – –) simulation of O–Al–Si–P–Rn–Te–Sr–V–K–Ge.

different to the transmission spectra (Fig. 7b). In this case the major species is paramagnetic and superparamagnetic Fe^{3+} similar to the C site present in the bulk sample, the Fe^{2+} percentage being very low.

Taking into account that both Fe^{3+} and Fe^{2+} ions could be related directly to the schiller surface effect of glass-ceramics obtained from muscovite–amblygonite mixtures, the muscovite containing approximately 2% Fe^{2+}, Mössbauer analyses have been carried out on both surface and bulk materials. On the other hand, iron is an easily diffusible element at higher temperatures, and hence can migrate to the material surface and be oxidized by the thermal treatment necessary for crystallization. Therefore, the Fe^{3+}/Fe^{2+} ratio on the surface changes with respect to the bulk material.

4. Discussion

The XRD diagrams previously obtained [1] showed that crystallization of muscovite–amblygonite glasses gives rise to β-spodumene solid solution. This fact is congruent with the situation of glass composition in the Li_2O–Al_2O_3–SiO_2 equilibrium phase diagram [10].

The general microstructure, observed by SEM, shows surface precipitation of very small crystals with a rounded shape as reported previously [11]. The degree of crystallization decreases from the surface to the bulk material.

This fact is related to the surface increment of iron such as was demonstrated by SEM/EDX microanalysis. The excessive migration of Fe^{3+} to the surface and cracking of the surface associated with spodumene can be controlled with the nucleating agent addition without suppressing the schiller effect as seen before [2]. The additives MgO, TiO_2 and ZrO_2 favour a more homogeneous crystallization controlling the excessive growth of crystals and, consequently, the Fe^{3+} solid solution into the β-spodumene. Both Ti^{4+} and Zr^{4+} partially substitute the Si^{4+} in the pyroxene structure of spodumene. Likewise, ZrO_2 inclusion is good for strengthening the spodumene matrix or the pyroxene solid solution.

This solid solution is lower according to the EPR analysis, following the sequence: TiO_2 > MgO > ZrO_2. In fact, the Li^+ and Si^{4+} could be substituted by

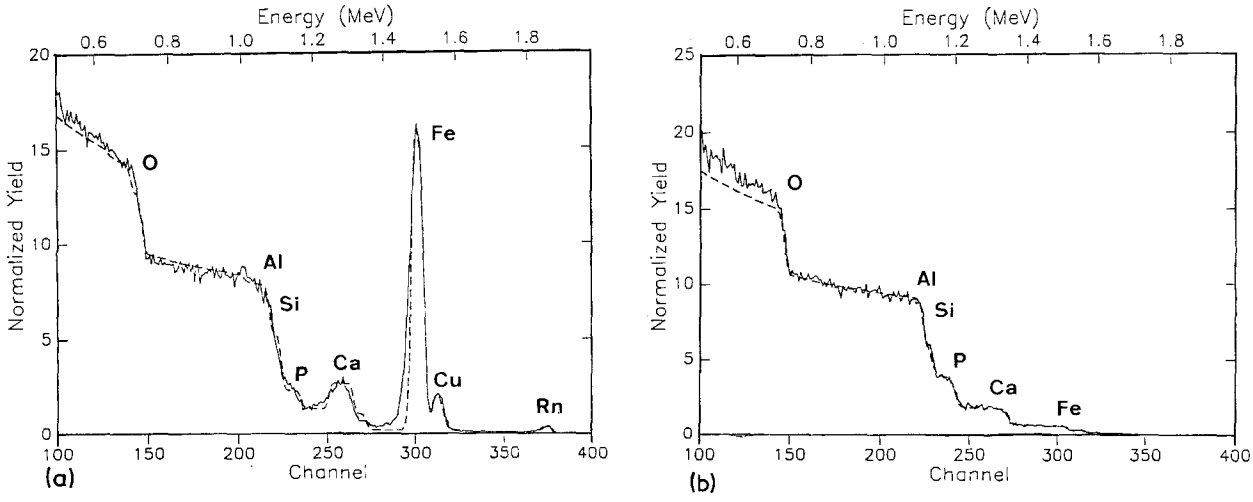

Figure 5 RBS spectra of the opaque glass-ceramic Ma2 obtained at 600° C for 16 h: (a) reflecting surface, and (b) back surface, whose reflecting surface was removed by grinding. (a) (——) Instituto de Ceramica, opaque, gic 01-08, (– – –) simulation of Fe–O–Al–Ca–Rn–Cu/O–Al–P–Ca–Rn–Te–Sr/O–Al–F. (b) (——) Instituto de Ceramica, opaque, gic 01-10, (– – –) simulation of Fe–O–Al–Ca–Rn–Cu–P–Sr–Si.

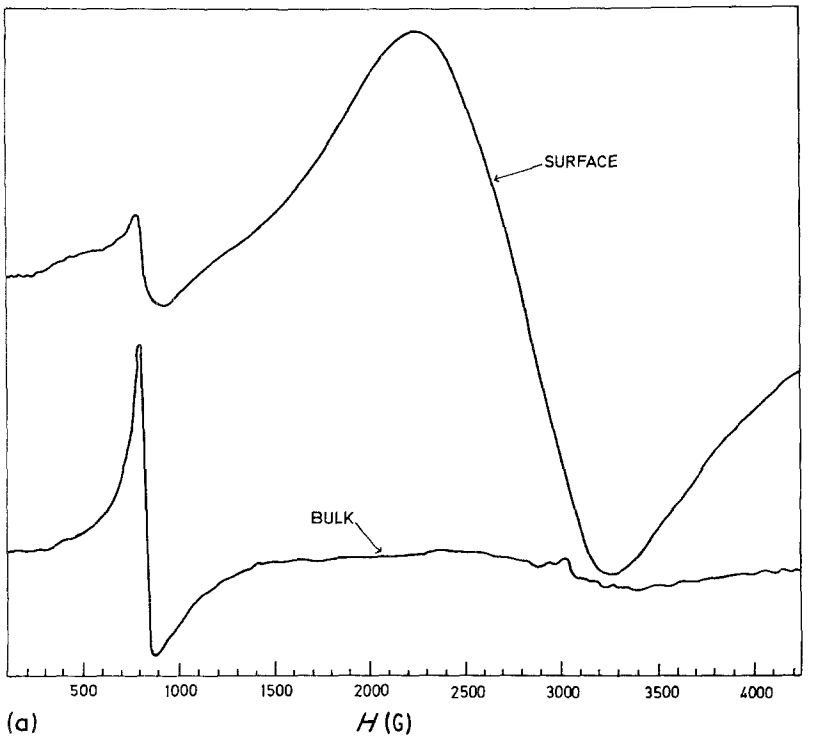

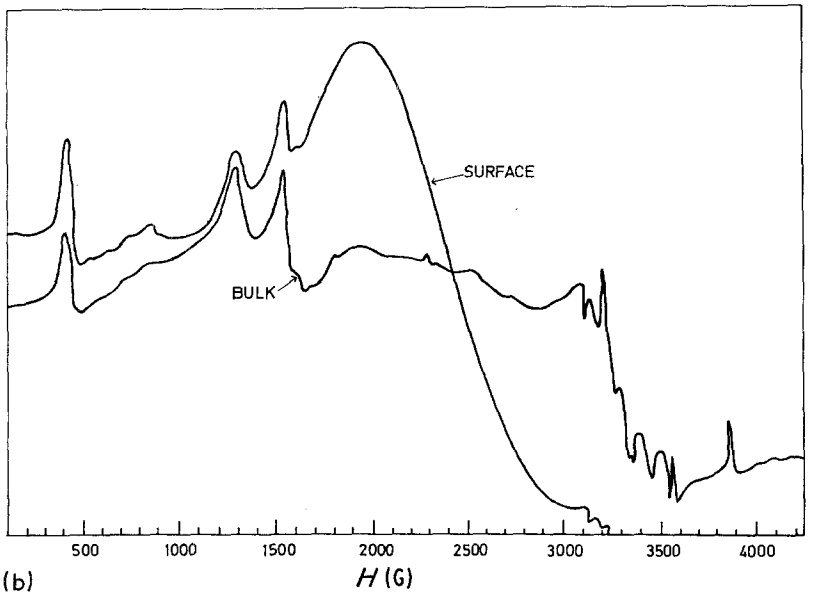

Figure 6 EPR spectra obtained on the surface and in the bulk of the Ma5 glass-ceramics obtained at 600° C for 16 h: (a) without additive; (b) with TiO_2 additions; (c) with MgO addition and (d) with ZrO_2 addition.

Fe^{2+} according to the following reaction:

$$2Li^{+} + Si^{4+} \rightleftarrows 3Fe^{2+} \quad (1)$$

In the pyroxene solid solution series, spodumene $LiAl(Si_2O_6)$ has a similar structure to the main representative of pyroxenes, diopside, with the formula $CaMg(Si_2O_6)$, where calcium and magnesium are exchanged for smaller ions like lithium and aluminium [12].

TABLE III EPR peak ratios for Fe^{3+} and Fe^{2+}: $R = I_{Fe^{3+}}/I_{Fe^{2+}}$ (EPR)

	R
Original glass-ceramics without additives	25
Glass ceramics plus:	
TiO_2	4.3
MgO	1.9
ZrO_2	1.5

Otherwise, the following substitutions can take place:

$$Al^{3+} + Si^{4+} \rightleftarrows 2Fe^{2+} + Fe^{3+} \quad (2)$$

and

$$Al^{3+} + Li^{+} \rightleftarrows Mg^{2+} + Mg^{2+} \quad (3)$$

Reaction 3 seems less probable with the former results, but Reaction 2 is confirmed by both reflection Mössbauer and EPR techniques. Thus, the EPR spectra show three bands due to Fe^{3+} isolated in the spodumene lattice (main crystalline phase) and another wide and intense band associated with Fe^{2+}.

TABLE IV Mössbauer parameters obtained from spectra

	QS (min sec^{-1})	IS (min sec^{-1})	I_x/I_{tot}
Fe^{2+} (A site)	2.44 ± 0.04	1.10 ± 0.02	0.47 ± 0.05
Fe^{2+} (B site)	1.92 ± 0.05	1.02 ± 0.03	0.41 ± 0.05
Fe^{3+} (C site)	0.60 ± 0.10	0.50 ± 0.07	0.12 ± 0.01

Figure 6 Continued.

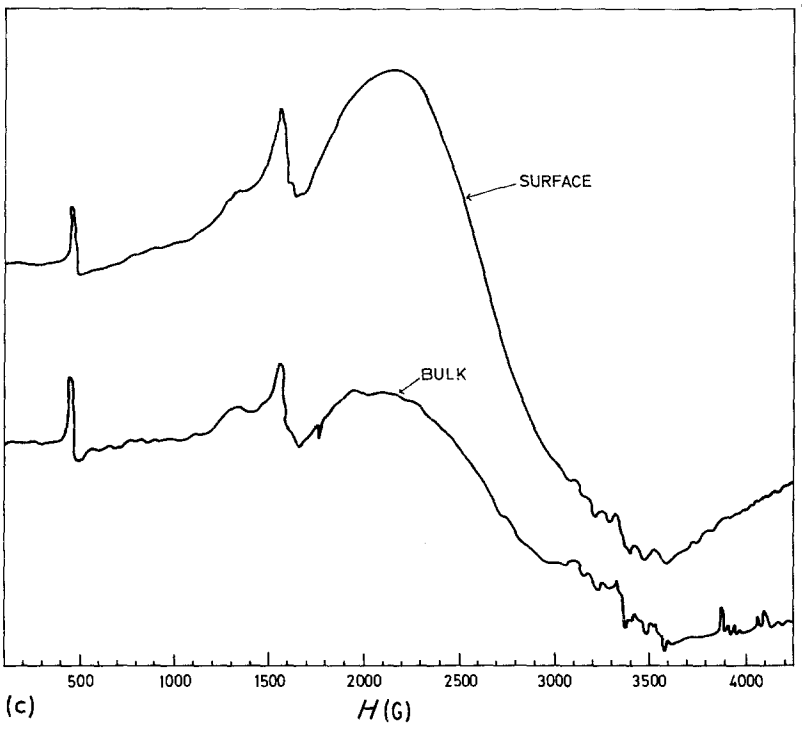

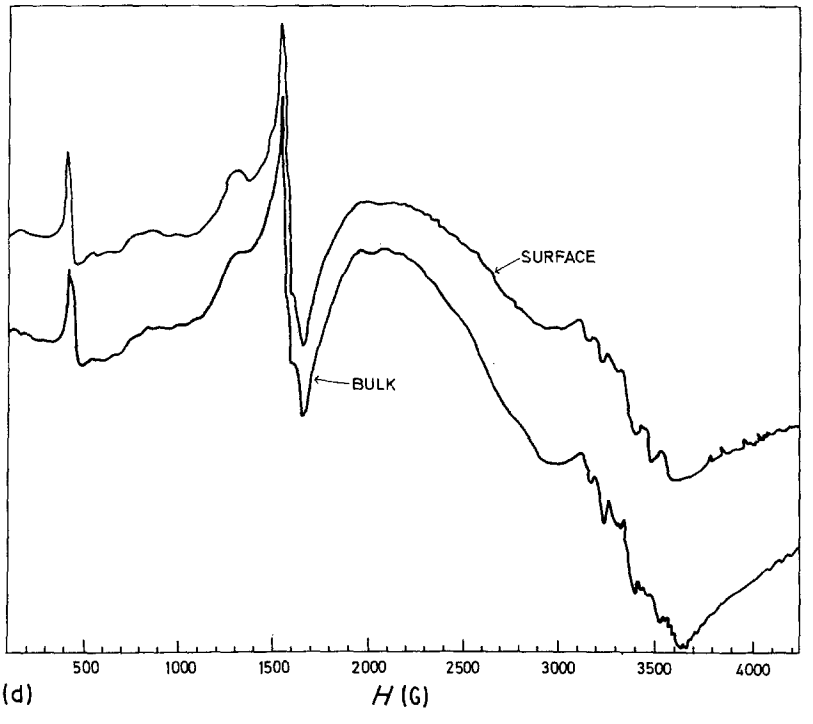

Similarly, in spodumene the substitution

$$2Li^{+} + Al^{3+} \rightleftarrows Fe^{3+} + Fe^{2+}$$

can give rise to a spodumene pyroxene with chain sliding, chain distortion and so a different structure, possibly even containing metallic cations.

This type of substitution can produce, in this case, surface crystallization in glass-ceramics similar to the aventurine or iridescent effects widely described in some minerals [13].

5. Conclusions

The surface analyses by ESCA, RBS, EPR and Mössbauer techniques performed on glass-ceramics showing reflecting surfaces such as aventurine, and obtained from muscovite–amblygonite original glasses, have been very valuable in elucidating the formation of the reflecting or schiller effects.

They showed that the glass composition close to the surface is significantly different from the bulk composition. Iron oxide has been enriched up to a concentration of $\sim 50\%$. Al_2O_3 is close to the bulk concentration, and SiO_2 and P_2O_5 are decreased. EPR surface and bulk analyses have shown that Fe^{3+} ions are associated with the spodumene structure and Mössbauer analysis confirms that the surface is enriched in Fe^{3+} ions. These Fe^{3+} ions substitute Al^{3+} in the β-spodumene solid solution.

Acknowledgements

We thank CAICYT for financial support, Professor Munuera and Gonzalez Elipe, University of Sevilla,

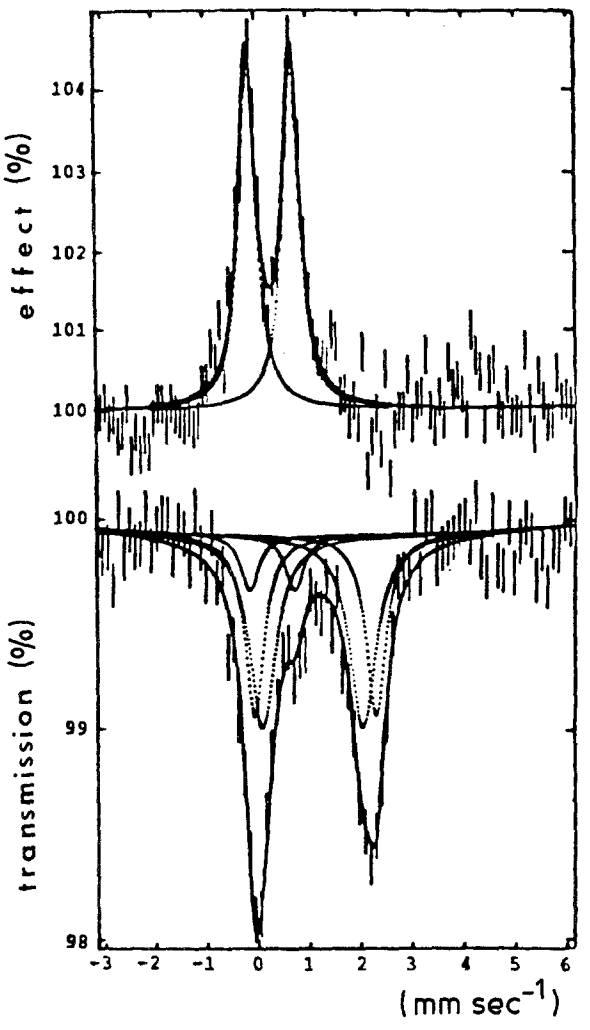

Figure 7 Mössbauer spectra obtained on the same Ma5 glass-ceramic as in Fig. 1: (a) reflected spectrum, and (b) transmitted spectrum.

for the ESCA-XPS analysis and to Dr Goretzi (Perkin-Elmer) and the General Ionex Corp (C. N. Sayers) for facilities in using the surface techniques. Valuable help from M. Gracia with Mössbauer analysis and J. Soria for EPR, is acknowledged. Finally, we thank A. J. Whitehead, Cambridge University, for carefully reviewing the paper.

References

1. J. Má RINCON, *Bol. Soc. Esp. Cerám. Vidr.* **23** (1984) 173.
2. P. CALLEJAS, Má F. BARBA and J. Má RINCON, *J. Mater. Sci. Lett.* **4** (1985) 1171.
3. R. BRÜCKNER, H. U. CHUN, H. GORETZKI, M. SAMMET, *J. Non-Crystal. Solids* **42** (1980) 49.
4. M. A. NICOLETT and W. K. CHU, *Amer. Lab.* March (1975) 8 pp.
5. J. WONG and C. A. ANGELL, "Glass Structure by Spectroscopy", (Marcel Dekker, New York, Basel, 1976) pp. 555–668.
6. R. H. SANDS, *Phys. Rev.* **99** (1955) 1222.
7. J. G. STEVENS *et al.*, "Handbook of Mineral Data Mössbauer", (Effect Data Center, University of North Carolina, 1983).
8. J. R. CANCEDO, M. GRACIA, P. CALLEJAS and J. Má RINCON, International Conference on the Application of the Mössbauer effect, edited by R. Coussement and G. Laugouche, 16–20 September, 1985, Leuven, Belgium.
9. G. WEYER, "Mössbauer Effect Methodology", Vol. 10, edited by Gruverman and Reidel (Plenum, New York, 1976) p. 301.
10. Q. Q. CHEN, P. L. GAI, G. W. GROVES, *J. Mater. Sci.* **17** (1982) 2671.
11. J. Má RINCON and P. CALLEJAS, Communication to the Annual Meeting of the Spanish Glass and Ceramic Society, Segovia, Spain (1985) to be published.
12. S. A. MORSE, "Basalts and Phase Diagrams" (Springer-Verlag, New York, Heidelberg, Berlin, 1980).
13. W. A. DEER, R. A. HOWIE and J. ZUSSMAN, "An Introduction to the Rock-Forming Minerals" (Longman, London, 1978) p. 334.

Received 26 May
and accepted 24 July 1987